International Journal on Magnetic Particle Imaging
Vol 3, No 1, Article ID 1703003, 9 Pages

Infinite Science Publishing

Research Article

Effect of particle size and structure on harmonic intensity of blood-pooling multi-core magnetic nanoparticles for magnetic particle imaging

Satoshi Ota[a,*] · Ryoji Takeda[b] · Tsutomu Yamada[b] · Ichiro Kato[c] · Satoshi Nohara[c] · Yasushi Takemura[b]

[a]Department of Electrical and Electronic Engineering, Shizuoka University, Hamamatsu, Japan
[b]Department of Electrical and Computer Engineering, Yokohama National University, Yokohama, Japan
[c]The Nagoya Research Laboratory, Meito Sangyo Co., Ltd., Kiyosu, Japan
*Corresponding author, email: ota.s@shizuoka.ac.jp

Received 25 November 2016; Accepted 23 January 2017; Published online 23 March 2017

Abstract

Magnetic particle imaging has been developed by the optimization of the tracer materials, excitation systems, and system functions for image reconstruction. Here, we prepared and studied magnetic nanoparticles with different core diameters, coated by carboxymethyl-diethylaminoethyl dextran as a blood-pooling agent. For comparison, measurements were also performed using Resovist®, a widely used tracer agent. Transmission electron microscopy analysis of the prepared samples of nanoparticles revealed monodisperse single-core, chainlike aggregation, and multi-core structures. For optimizing the core size and structure of magnetic nanoparticles for use as imaging tracers, we evaluated the magnetization response to an applied field and harmonic intensity by measuring direct and alternating current hysteresis loops. To evaluate the dependence of the harmonic intensity on the core size and particle structures, large-magnetization particles were assembled using magnetic separation. The harmonic intensity depended not only on the core size but also on the particle structure. Diameters and distributions of single- and multi-core particles are important parameters. Solid and liquid samples of particles were studied for characterization of imaging of solid objects (such as tumors and organs) and liquids (such as blood).

I. Introduction

Magnetic particle imaging (MPI) is an imaging technique for visualization of magnetic nanoparticles (MNPs) in the human body [1]. The signal owing to the MNPs tracer is similar to that generated at the air-tissue interface in magnetic resonance imaging (MRI) [2]. A typical MPI system reports the harmonic signal generated by MNPs. Thus, compared with MRI, MPI does not suffer from the problem of false detection. In particular, a protocol for in vivo measurements has been recently developed for MPI [2–5]. In addition, the possibility of multi-color MPI, using different types of MNPs, was considered [6].

To enhance the MPI signal intensity, it is necessary to understand how the structural properties of MNPs affect the signal intensity. The dependence of the MPI signal on the core diameter and anisotropy of MNPs was investigated [7, 8]. In those conventional studies, large-core

particles, exhibiting ferromagnetism, generated a strong MPI signal. The distribution of the particle core diameter also affected the intensity of the MPI signal [9, 10]. The MPI signal increased after magnetically separating large-magnetization MNPs [10]. To detect specific organs and cancer tissues, MNPs were functionalized using targeting agents. The MPI signals of the functionalized MNPs were measured and the targeting ability of the MNPs was confirmed by performing in vivo and in vitro experiments [11, 12].

In the present study, we evaluated the harmonic intensities of MNPs with different core diameter and particle structure, by measuring their magnetization responses to direct current (DC) and alternating current (AC) magnetic fields. The measured MNPs were functionalized using a blood-pooling agent [13]. Moreover, to assemble the particles with large magnetization, magnetic separation was performed. To consider the capacity of the prepared MNPs to serve as the MPI tracer, the results were compared with those obtained using Resovist®, a widely used material for the studies of MPI.

II. Material and Methods

II.I. Materials and Sample Preparation

Experiments were performed using water-based maghemite nanoparticles (CMEADM-004, CMEADM-023, CMEADM-033, and CMEADM-033-02), and Resovist®. The nanoparticles of the CMEADM series were supplied by Meito Sangyo Co. LTD., Kiyosu, Japan. Resovist® was distributed by FUJIFILM RI Pharma Co., Ltd., Tokyo, Japan. The nanoparticles of the CMEADM series were coated by carboxymethyl-diethylaminoethyl dextran, and their core and hydrodynamic diameters are listed in Tab. 1. Carboxymethyl-diethylaminoethyl dextran-coated iron oxide nanoparticles are negatively charged and are used as a blood-pooling contrast agent [13]. In addition, CMEADM-033-02 was prepared by magnetically separating large-magnetization MNPs from CMEADM-033. The measured samples were divided into solid and liquid samples. In the solid samples, MNPs were fixed with agar, at the concentration of 28 mg-Fe/mL. In the liquid samples, MNPs were dispersed in water, at the concentration of 28 mg-Fe/mL. The samples were encapsulated in 10 mm diameter cylindrical tubes. The saturation magnetizations of the measured MNPs were estimated by fitting the measured DC major hysteresis loops to the magnetization curve calculated using the Langevin function in the field intensity above 560 kA/m.

II.II. Measurements

DC hysteresis loops were measured using a vibrating sample magnetometer (VSM) at room temperature. The intensities of the DC excitation fields were 0–800 kA/m and 0–8 kA/m, for the major and minor hysteresis loops, respectively. AC hysteresis loops and harmonic signals were measured using a detection circuit that consisted of pick-up and cancel coils located in an excitation coil [14]. The frequencies and the maximal intensities of the AC excitation fields were 1–100 kHz and 8 kA/m, respectively.

Table 1: Core diameter d_C, hydrodynamic diameter d_H, and saturation magnetization M_S, for the measured MNPs.

Measured MNP	d_C [nm]	d_H [nm]	M_S [Am^2/kg-Fe]
CMEADM-004	4	38	98
CMEADM-023	8	83	113
CMEADM-033	5–6	54	104
CMEADM-033-02	6	64	119
Resovist®	5	75	96

III. Results and Discussion

III.I. Particle Structure

Fig. 1(a)–(e) show the transmission electron microscopy (TEM) images for CMEADM-004, CMEADM-023, CMEADM-033, CMEADM-033-02, and Resovist®, respectively. The measured MNPs were divided into three categories based on their structure: monodispersed single-core particles, aggregated chain particles, and aggregated multi-core particles (Fig. 1). Tab. 2 shows the structures for the different categories of the measured MNPs, for the TEM data in Fig. 1. The clustered single-domain particle is the multi-core particle, and it prevents other particles from sedimentation by large aggregation [15]. The aggregated diameter of the multi-core particle is effectively equal to the core diameter of the multi-core particle, such as the core diameter of the single-core particle [16]. It was shown that both single- and multi-core particles consist of Resovist® [16, 17].

Table 2: The structures formed by the measured MNPs. The + and - signs indicate whether the structure is or is not detected by TEM in Fig. 1.

Measured MNP	Singlecore	Chain	Multicore
CMEADM-004	+	-	+
CMEADM-023	-	+	+
CMEADM-033	+	+	+
CMEADM-033-02	+	+	+
Resovist®	+	-	+

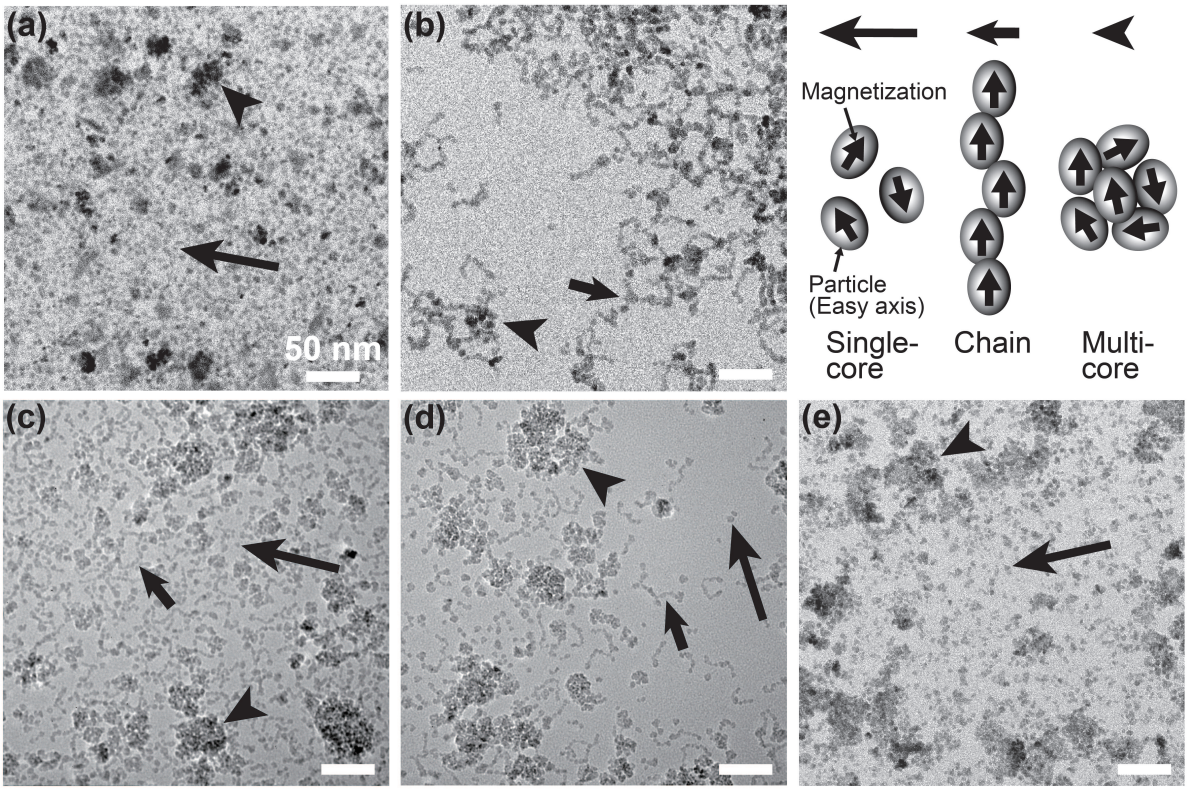

Figure 1: TEM images of the measured MNPs. (a)–(e) The images of CMEADM-004, CMEADM-023, CMEADM-033, CMEADM-033-02, and Resovist®. The long arrows, short arrows, and arrow heads show the single-core, chain, and multi-core structures, respectively. The scale bar is 50 nm.

III.II. DC Magnetization Properties

Fig. 2(a) and Fig. 2(b) show the DC major hysteresis loops for the solid and liquid samples, respectively. The insets in Fig. 2 show the magnified images of the major hysteresis loops, for low field intensities. Fig. 3(a) and Fig. 3(b) show the DC minor hysteresis loops for the solid and liquid samples, respectively. The insets in Fig. 3 show the magnified images of the corresponding hysteresis loops, around the origin. For the solid samples, CMEADM-004 and CMEADM-023, and Resovist® exhibited marginal coercivity, indicating superparamagnetic behavior. In contrast, CMEADM-033 and CMEADM-033-02 exhibited coercivity, indicating ferromagnetic behavior. The coercivity of CMEADM-033 was lesser than that of CMEADM-033-02 because the core particles in the case of CMEADM-033 were smaller than those in the case of CMEADM-033-02. Large core diameters induced high anisotropic energy, affecting the coercivity. For the liquid samples, all MNPs exhibited marginal coercivity because ferromagnetic nanoparticles also exhibited superparamagnetic behavior, owing to the rotation of the easy axis [18]. The rotation of the easy axis reduced the anisotropic energy.

For CMEADM-004, CMEADM-023, and CMEADM-033, the magnetizations increased with increasing the core diameter, for both the solid and liquid samples (Fig. 2 and Fig. 3). The magnetization of CMEADM-033-02 was higher than that of CMEADM-023, despite the larger core diameter of CMEADM-023 (Fig. 2(a) and Fig. 3(a)). As mentioned above, in the case of CMEADM-033-02, the core particles with small magnetization (reflecting relatively small core diameters and deteriorated crystalline structure) were removed using magnetic separation. Thus, not only the core diameter but also the structure of the magnetic crystal (obtained during synthesis) is important for enhancing the magnetization of particles. For field intensities corresponding to minor hysteresis loops, the magnetization of Resovist® was higher than that of CMEADM-023, for the solid samples (Fig. 3(a)). However, for field intensities in Fig. 2(a), the magnetization of Resovist® was lower than that of CMEADM-023, along with the saturation magnetization (Tab. 1). Moreover, the magnetization of Resovist® was higher than that of CMEADM-033 for field intensities up to 150 kA/m for the solid sample, and for field intensities up to 50 kA/m for the liquid sample (Fig. 2(a) and Fig. 2(b)). However, in addition to the saturation magnetization, the magnetization of Resovist® for field intensities above ~150 kA/m for the solid sample and

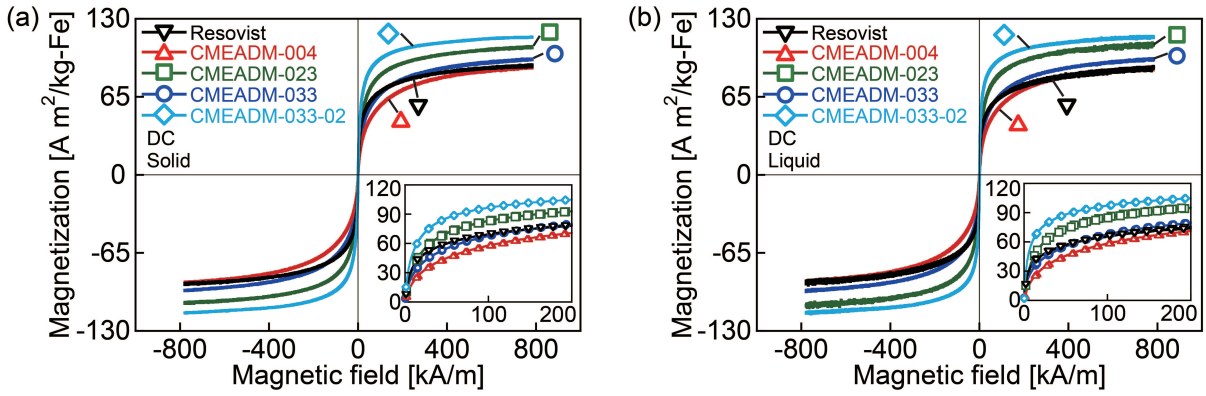

Figure 2: The DC major hysteresis loops of the measured MNPs for (a) the solid and (b) the liquid samples. The applied field intensity was in the 0–800 kA/m range. The insets show the magnified images of the major hysteresis loops at low- intensity fields.

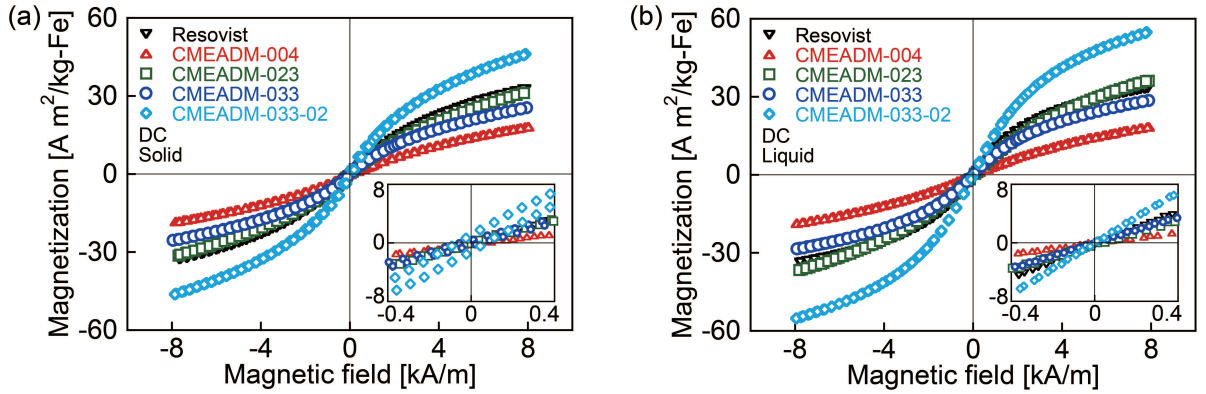

Figure 3: The DC minor hysteresis loops of the measured MNPs for (a) the solid and (b) the liquid samples. The applied field intensity was in the 0–8 kA/m range. The insets show the magnified images of hysteresis loops around the origin.

above ~50 kA/m for the liquid sample was lower than that of CMEADM-033. Tab. 2 shows that multi-core particles were obtained not only for Resovist® but also for all other measured MNPs. Except for the chain structure, the particle magnetizations were determined by the ratios of single-core and multi-core particles, and the distribution of core and effective core diameters, respectively. The saturation magnetization depended on the core diameter, and the effective core diameter affected the magnetization process, in particular for low field intensities.

However, magnetization of particles depends not only on the mean core diameter, but is also affected by the distributions of core diameter and crystalline structures. The saturation magnetization of CMEADM-033-02 was the highest across all measured MNPs, despite the fact that the mean core diameter of CMEADM-033-02 was smaller than that of CMEADM-023, because large-magnetization core particles, derived from the crystalline structure, were purified using magnetic separation. On the other hand, for low field intensities, the magnetization of Resovist® was higher than those of CMEADM-023 and CMEADM-033, whereas the saturation magnetization of Resovist® was lower than those of CMEADM-023 and CMEADM-033. This indicates that the distribution ratio of multi-core particles in Resovist® was higher than those in CMEADM-023 and CMEADM-033. Moreover, the magnetization of CMEADM-033-02 was larger than that of Resovist®, regardless of the field intensity. This indicates that, in addition to the large core diameter of CMEADM-033-02 (compared with Resovist®), the distribution ratio of multi-core particles to single-core particles for these MNPs is relatively high, compared with other scenarios, owing to the purification using magnetic separation. The magnetization for low field intensities was particularly affected by the distribution ratio of multi-core particles and their effective core diameters. This is in agreement with previous results, according to which, for multi-core particles, the magnetization of the effective core particle is determined by a low field intensity, while the magnetization of the core nanocrystal is determined by the saturation magnetization and the volume

of the core particle [19].

For the liquid samples, the magnetizations of CMEADM-023, CMEADM-033, and CMEADM-033-02 were increased compared with those for the solid samples, whereas the magnetizations of CMEADM-004 and Resovist® for the liquid samples slightly increased compared with those for the solid samples. TEM observations revealed that the CMEADM-023, CMEADM-033, and CMEADM-033-02 samples contained core particles with the chain structure (Fig. 1). In contrast, CMEADM-004 and Resovist® did not exhibit this chain structure. The chain structure yielded large dipole interactions among adjacent particles owing to the uniaxial magnetization alignment. The experimental measurements and numerical simulations revealed the positive and negative effects of the dipole interactions among the particles in the chain structure on the magnetization; these effects depended on the applied field's intensity and particle parameters, such as the core diameter and anisotropy [20–22]. At low field intensity, the chain structure decreases the magnetization in the solid samples because dipole interactions effectively increase the particle anisotropy [21]. On the other hand, in the liquid samples, the effective easy axis formed by the chain structure rotates with aligning the magnetization direction to the direction of the applied field. The magnetizations of each core particle consisted in the chain structure are fixed by the dipole interactions. When the easy axis formed by the chain structure is rotatable, the magnetizations aligned by the dipole interactions rotate as the effectively single magnetization as with the effective core of the multi-core structure. The rotation of the easy axis increases the magnetization owing to a reduction in the anisotropic energy [23]. The magnetization of particles with high anisotropic energy increases more strongly for the liquid samples compared with the magnetization in the solid samples, because the magnetization of highly anisotropic particles is strongly determined by the easy axis. In Fig. 3, the magnetization of CMEADM-033-02 in the liquid sample was significantly higher than that in the solid sample. In the liquid sample, the magnetization of ferromagnetic nanoparticles can be rotated by applying an external field because the easy axis is rotated owing to the magnetic torque induced by the rotation of the magnetization [24]. The particles distributed in CMEADM-033-02 exhibit a somewhat ferromagnetic behavior, manifested as the largest coercivity across all measured MNPs.

III.III. AC Magnetization Properties

Fig. 4(a) and Fig. 4(b) show the AC minor hysteresis loops for the maximal field intensity of 8 kA/m, at the field frequency of 10 kHz, for the solid and liquid samples, respectively. For these AC minor hysteresis loops, the relative order of maximal magnetizations across the measured MNPs was similar to that obtained for the DC minor hysteresis loops in Fig. 3. For both the solid and liquid samples, the maximal magnetization of CMEADM-033-02 was the highest across all of the measured MNPs, owing to the high distribution ratio of multi-core particles, in addition to purified core particles in terms of the core diameter and magnetic crystalline structure, as obtained by magnetic separation. The maximal magnetizations of CMEADM-004, CMEADM-023, and CMEADM-033 depended on their core diameters. The maximal magnetization of Resovist® was higher than those of CMEADM-023 and CMEADM-033 for the solid samples. For the liquid samples, the maximal magnetization of Resovist® was higher than that of CMEADM-033 and lower than that of CMEADM-023. The large magnetization derived from the large core diameter in the case of CMEADM-023 was inhibited by a strong dipole interaction derived from the chain structure in the solid samples.

The insets in Fig. 4 show the magnified images of the samples' AC minor hysteresis loops around their coercivity regions. For the AC hysteresis loop of a sample, the coercivity was obtained from the phase delay of the sample's magnetization compared to an applied external magnetic field. Fig. 5 shows the dependence of the phase delay on the field frequency for the solid and liquid samples. In Fig. 4, the MNPs with large phase delays exhibit high coercivities. The phase delay is associated with the magnetic relaxation time [25]. When the cycle of the applied field is longer than the relaxation time, the resulting phase delay is small because the rotation of the magnetization follows the change in the field. Magnetic relaxation consists of the Néel and Brownian relaxations, associated with the magnetization and easy axis responses to the applied field, respectively. The Néel relaxation time τ_N and the Brownian relaxation time τ_B are given by

$$\tau_N = \tau_0 e^{\frac{KV_M}{k_B T}}, \tag{1}$$

$$\tau_B = \frac{3\eta V_H}{k_B T}, \tag{2}$$

where τ_0 is the attempt time of $\sim 10^{-9}$ s (associated with gyromagnetic procession), K is the magnetic anisotropic constant, V_M is the volume of the core particle, k_B is the Boltzmann constant ($1.38 \cdot 10^{-23}$ J/K), T is the temperature in Kelvins, η is the viscosity, and V_H is the volume of the hydrodynamic particle [26, 27].

The Néel relaxation time increases with increasing core diameter (Eq. (1)). For the solid samples, the phase delay of CMEADM-023 was slightly larger than that of CMEADM-004, because the core diameter of CMEADM-023 is larger than that of CMEADM-004. The slight phase delay difference between CMEADM-004 and CMEADM-023 was caused by a much longer cycle of the applied field than the Néel relaxation time of both CMEADM-004 and CMEADM-023, for the measured field frequencies.

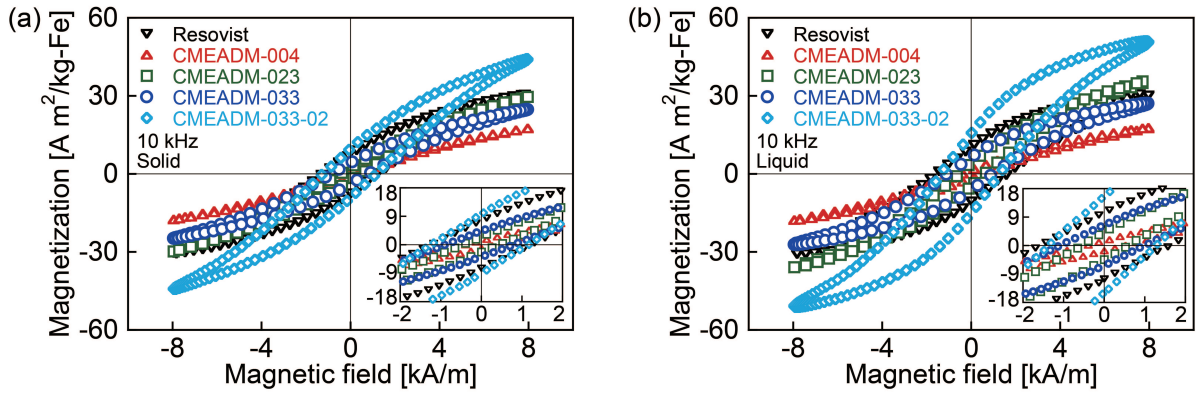

Figure 4: The AC minor hysteresis loops of the measured MNPs for the (a) the solid and (b) the liquid samples. The maximal applied field intensity was 8 kA/m. The field frequency was 10 kHz. The insets show the magnified images around the coercivities.

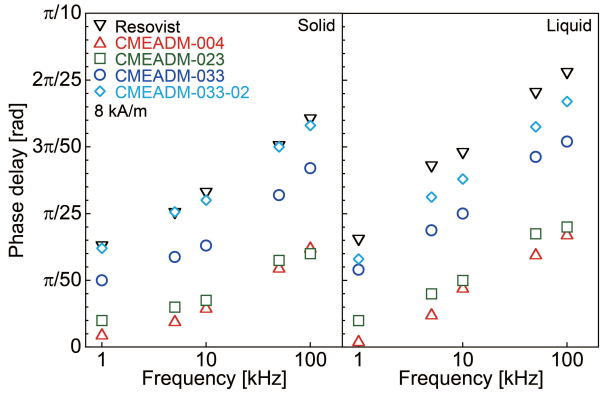

Figure 5: The dependence of the phase delay of the magnetization of the measured MNPs on the field frequency, for the solid and liquid samples. The maximal applied field intensity was 8 kA/m.

The phase delay of CMEADM-033 was larger than that of CMEADM-023, whereas the core diameter of CMEADM-033 was smaller than that of CMEADM-023. Considering the diameters and distributions of single- and multi-core particles, the total core diameter was larger for CMEADM-033 compared with CMEADM-023. Therefore, the Néel relaxation time was affected by the diameters and distributions of both the single- and multi-core particles. The phase delays for CMEADM-033-02 and Resovist® were larger than that for CMEADM-033. This also indicates that the total core diameters for CMEADM-033-02 and Resovist® were larger than that for CMEADM-033. In particular, considering the larger core diameter of CMEADM-033 than that of Resovist®, this agrees with the large magnetization of Resovist® at low field intensities, compared with the magnetization of CMEADM-033 in Fig. 2 and Fig. 3. The phase delay for CMEADM-033-02 was similar to that for Resovist®. This indicates that the total core diameter for CMEADM-033-02 was similar to that for Resovist®.

For field frequencies above 5 kHz, the phase delays of all the measured MNPs for the liquid samples were larger than those for the solid samples, owing to the Brownian relaxation. For the field frequency of 1 kHz, the difference in the phase delays between the solid and liquid samples was marginal. When the cycle of the applied field is longer than the Brownian relaxation time, the phase delay for the liquid sample is similar to or smaller than that for the solid sample [18, 28]. The values of the Brownian relaxation times calculated from Eq. (2) and the hydrodynamic diameters in Tab. 1 were 19 μs, 190 μs, 54 μs, 89 μs, and 140 μs, for CMEADM-004, CMEADM-023, CMEADM-033, CMEADM-033-02, and Resovist®, respectively. Previously, the effect of Brownian relaxation was observed with respect to the measured MNPs of the Brownian relaxation time of 48 μs [18]. Thus, the increase in the magnetization for the liquid samples compared with that for the solid samples was owing to the rotation of the easy axis, because in the liquid samples, Brownian relaxation occurred in addition to the Néel relaxation [23]. In the case of the measured MNPs, the Néel relaxation time was shorter than Brownian relaxation time. Thus, the easy axis was rotated with the delay from the rotation of the magnetization.

III.IV. Harmonics Measurements

Fig. 6 shows the intensities of the odd-numbered harmonics, for the solid and liquid samples. Fig. 7 shows the dependence of the intensity of the third harmonic normalized by the intensity of the fundamental harmonic, M_3/M_1, on the field frequency, for the solid and liquid samples. This normalized quantity reveals that the linearity of the magnetization process in the measured MNPs independent of the saturation magnetization. With respect to the solid samples, the intensities of both the fundamental and higher-order harmonics were higher for CMEADM-023 compared with CMEADM-004, because the core diameter of CMEADM-023 was larger

than that of CMEADM-004. However, for CMEADM-023 M_3/M_1 was similar to that for CMEADM-004. The non-linear behavior of magnetization for CMEADM-023 was similar to that for CMEADM-004, despite the larger core diameter of CMEADM-023. The high anisotropy of the chain structure inhibited the steep increase in the magnetization at low field intensities. The harmonic intensities for CMEADM-033 were slightly higher than those for CMEADM-023, whereas the fundamental intensity for CMEADM-033 was lower than that for CMEADM-023. Moreover, for all harmonics down to the ninth harmonic, the harmonic intensities for CMEADM-033-02 were lower than those for CMEADM-033, even though the harmonic intensities for CMEADM-033-02 were higher than those for CMEADM-033 for up to seventh harmonic. In addition, M_3/M_1 for CMEADM-033 was higher than that for CMEADM-023 and CMEADM-033-02. These results indicate that the non-linear behavior of magnetization for CMEADM-033 was higher than that for CMEADM-023 and CMEADM-033-02. It is indicated that the ratio of the multi-core particles in CMEADM-023 was lower than that in CMEADM-033. The ratio of the multi-core particles particularly affects the magnetization at the low field intensity. When the magnetization steeply increased, the process was quasi-linear. Thus, the magnetization of multi-core particles in CMEADM-033-02 exhibited quasi-linearity because the applied field intensity was not sufficiently high to ensure a sufficient reduction of the derivative of the magnetization of multi-core particles with respect to the field intensity. The derivative of the magnetization with respect to the field intensity was measured for evaluating the nonlinear behavior of the magnetization [8].

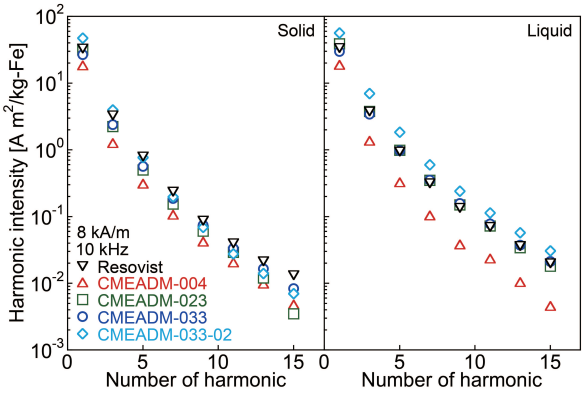

Figure 6: Harmonic intensities for odd-numbered harmonics, for the measured MNPs, for the solid and liquid samples. The maximal applied field intensity was 8 kA/m. The field frequency was 10 kHz.

For the liquid samples, the harmonic intensities of CMEADM-023, CMEADM-033, and CMEADM-033-02 were significantly higher than those for the solid samples (Fig. 6 and Fig. 7). The magnetization of the liquid

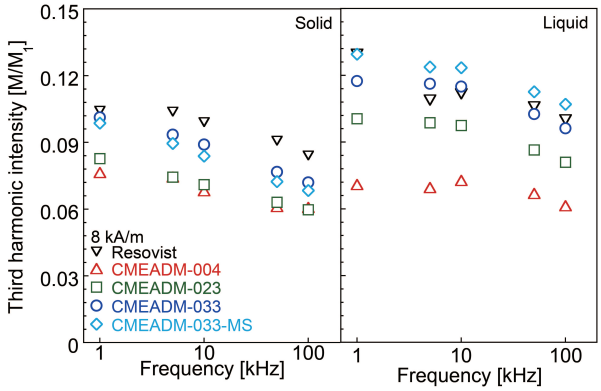

Figure 7: Intensity of the third harmonic, normalized by the intensity of the fundamental harmonic vs. the field frequency, for the measured MNPs, for the solid and liquid samples. The maximal applied field intensity was 8 kA/m.

samples increased because the rotation of the easy axis decreased the anisotropic energy. The chain structure of these MNPs exhibited high anisotropy. Owing to the rotation of the easy axis, the magnetization of these high-anisotropy particles steeply increased at low field intensities. This agrees with the magnetization response to the applied field, shown in Fig. 3. In addition, for the liquid samples, the M_3/M_1 of CMEADM-033-02 was higher than that of CMEADM-033, whereas for the solid samples the M_3/M_1 of CMEADM-033-02 was lower than that of CMEADM-033. This indicates that the large effective core diameter of the multi-core particles assembled by the magnetic separation also caused high anisotropy energy for CMEADM-033-02.

For Resovist®, the harmonic intensities down to the fifth harmonic were the highest across all measured MNPs in the solid samples, despite the low saturation magnetization associated with the small core diameter (Fig. 6 and Tab. 1). The high harmonic intensity of Resovist® is also manifested by the high M_3/M_1, shown in Fig. 7. The large effective core diameter of multi-core particles in Resovist® affected the non-linear response of magnetization associated with high M_3/M_1 [10]. Both the harmonic intensities and M_3/M_1 of Resovist® for the liquid sample were higher than those for the solid sample (Fig. 6 and Fig. 7). The anisotropic energy derived from the easy axis of core particles and dipole interaction of multi-core particles inhibited the magnetization, similar to what occurred for the chain structure. However, for Resovist®, the change between both the harmonic intensities and M_3/M_1 for the solid sample, and those for the liquid sample was smaller than the corresponding changes for CMEADM-023, CMEADM-033, and CMEADM-033-02, which is also shown in Fig. 8. Tab. 2 shows that the chain structure was not detected in Resovist®, and it was consisted in CMEADM-023, CMEADM-033, and CMEADM-033-02. Thus, rotation

of the easy axis for the liquid samples induced a steep increase in the magnetization at low field intensities. In particular, the harmonic intensity significantly increased owing to the chain structure of core particles in the liquid samples.

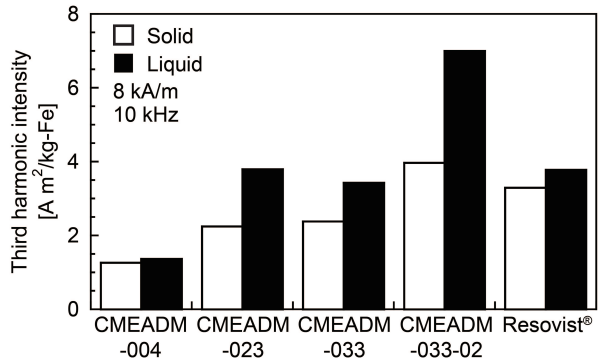

Figure 8: Intensity of the third harmonic, for the measured MNPs, for the solid and liquid samples. The intensity and the frequency of the applied field were 8 kA/m and 10 kHz, respectively. This graph shows the highlighted data in terms of the third harmonic in Fig. 6.

Fig. 8 shows M_3 for the measured MNPs for the solid and liquid samples in Fig. 6. For CMEADM-033-02, M_3 was ∼ 1.2 and ∼ 1.9 fold higher than those for Resovist® for the solid and liquid samples, respectively (Fig. 8). When the easy axis was rotatable, the M_3 value for CMEADM-033-02 was significantly higher than that for Resovist®. In addition, the M_3 values for CMEADM-033-02 were 1.7 and 2.0 fold higher than those for CEMADM-033, for the solid and liquid samples, respectively (Fig. 8). This trend was the same as the relationship between CMEADM-033-02 and Resovist®. For CMEADM-033-02, large particles with chain and multi-core structures assembled using magnetic separation exhibited a high anisotropic energy, owing to the dipole interactions in the solid samples. In contrast, the inhibition by the anisotropic energy was reduced and the magnetization steeply increased in the liquid samples. It was determined that the MPI signal increases with increasing the ratio of multi-core particles to single-core particles [17]. However, the particularly significant difference between the solid and liquid samples in the case of CMEADM-033-02 was attributed to large dipole interactions owing to the chain structure. Therefore, the chain structure amplifies the difference between the magnetization properties in the liquid vs. the solid samples, with respect to harmonics.

IV. Conclusion

We prepared and studied blood-pooling magnetic nanoparticles of different core diameters for MPI. The dynamics of magnetization at high field intensities (such that the saturation magnetization) were determined by the core diameter of single-core structures. On the other hand, the characteristics of magnetization at low field intensities (around the drive field intensity for MPI) were influenced by the effective core diameter of multi-core structures. Moreover, for the measured MNPs, TEM revealed the presence of the chain structure, in addition to the single- and multi- core structures. The chain structure exhibited strong anisotropy owing to dipole interactions among uniaxially aligned particles. Thus, the chain structure inhibits the harmonic intensity owing to the fixation of magnetization to the easy axis when the easy axis is not rotatable (e.g., for solid states such as tumors and organs). However, in a liquid (such as blood), the harmonic intensity is significantly higher because the magnetization is enhanced owing to the rotation of the easy axis formed by the chain structure.

References

[1] B. Gleich and J. Weizenecker. Tomographic imaging using the nonlinear response of magnetic particles. *Nature*, 435(7046):1214–1217, 2005. doi:10.1038/nature03808.

[2] B. Zheng, M. P. von See, E. Yu, B. Gunel, K. Lu, T. Vazin, D. V. Schaffer, P. W. Goodwill, and S. M. Conolly. Quantitative Magnetic Particle Imaging Monitors the Transplantation, Biodistribution, and Clearance of Stem Cells In Vivo. *Theranostics*, 6(3):291–301, 2016. doi:10.7150/thno.13728.

[3] J. Weizenecker, B. Gleich, J. Rahmer, H. Dahnke, and J. Borgert. Three-dimensional real-time in vivo magnetic particle imaging. *Phys. Med. Biol.*, 54(5):L1–L10, 2009.

[4] P. Vogel, M. A. Rückert, P. Klauer, W. H. Kullmann, P. M. Jakob, and V. C. Behr. First in vivo traveling wave magnetic particle imaging of a beating mouse heart. *Phys. Med. Biol.*, 61(18):6620–6634, 2016. doi:10.1088/0031-9155/61/18/6620.

[5] M. G. Kaul, O. Weber, U. Heinen, A. Reitmeier, T. Mummert, C. Jung, N. Raabe, T. Knopp, H. Ittrich, and G. Adam. Combined Preclinical Magnetic Particle Imaging and Magnetic Resonance Imaging: Initial Results in Mice. *Fortschr. Röntgenstr.*, 187(05): 347–352, 2015. doi:10.1055/s-0034-1399344.

[6] J. Rahmer, A. Halkola, B. Gleich, I. Schmale, and J. Borgert. First experimental evidence of the feasibility of multi-color magnetic particle imaging. *Phys. Med. Biol.*, 60(5):1775–1791, 2015. doi:10.1088/0031-9155/60/5/1775.

[7] R. M. Ferguson, A. P. Khandhar, S. J. Kemp, H. Arami, E. U. Saritas, L. R. Croft, J. Konkle, P. W. Goodwill, A. Halkola, J. Rahmer, J. Borgert, S. M. Conolly, and K. M. Krishnan. Magnetic Particle Imaging With Tailored Iron Oxide Nanoparticle Tracers. *IEEE Trans. Med. Imag.*, 34(5):1077–1084, 2015. doi:10.1109/TMI.2014.2375065.

[8] A. Tomitaka, R. M. Ferguson, A. P. Khandhar, S. J. Kemp, S. Ota, K. Nakamura, Y. Takemura, and K. M. Krishnan. Variation of Magnetic Particle Imaging Tracer Performance With Amplitude and Frequency of the Applied Magnetic Field. *IEEE Trans. Magn.*, 51(2):6100504, 2015. doi:10.1109/TMAG.2014.2341570.

[9] D. Eberbeck, F. Wiekhorst, S. Wagner, and L. Trahms. How the size distribution of magnetic nanoparticles determines their magnetic particle imaging performance. *Appl. Phys. Lett.*, 98(18):182502, 2011. doi:10.1063/1.3586776.

[10] T. Yoshida, N. B. Othman, and K. Enpuku. Characterization of magnetically fractionated magnetic nanoparticles for magnetic particle imaging. *J. Appl. Phys.*, 114(17):173908, 2013. doi:10.1063/1.4829484.

[11] H. Arami, A. P. Khandhar, A. Tomitaka, E. Yu, P. W. Goodwill, S. M. Conolly, and K. M. Krishnan. In vivo multimodal magnetic particle imaging (MPI) with tailored magneto/optical contrast agents. *Biomaterials*, 52:251–261, 2015. doi:10.1016/j.biomaterials.2015.02.040.

[12] A. Tomitaka, H. Arami, S. Gandhi, and K. M. Krishnan. Lactoferrin conjugated iron oxide nanoparticles for targeting brain glioma cells in magnetic particle imaging. *Nanoscale*, 7(40):16890–16898, 2015. doi:10.1039/c5nr02831k.

[13] N. Nitta, K. Tsuchiya, A. Sonoda, S. Ota, N. Ushio, M. Takahashi, K. Murata, and S. Nohara. Negatively charged superparamagnetic iron oxide nanoparticles: a new blood-pooling magnetic resonance contrast agent. *Jpn. J. Radiol.*, 30(10):832–839, 2012. doi:10.1007/s11604-012-0133-0.

[14] H. Kobayashi, A. Hirukawa, A. Tomitaka, T. Yamada, M. Jeun, S. Bae, and Y. Takemura. Self-heating property under ac magnetic field and its evaluation by ac/dc hysteresis loops of $NiFe_2O_4$ nanoparticles. *J. Appl. Phys.*, 107(9):09B322, 2010. doi:10.1063/1.3355936.

[15] S. Dutz, J. H. Clement, D. Eberbeck, T. Gelbrich, R. Hergt, R. Müller, J. Wotschadlo, and M. Zeisberger. Ferrofluids of magnetic multicore nanoparticles for biomedical applications. *J. Magn. Magn. Mater.*, 321(10):1501–1504, 2009. doi:10.1016/j.jmmm.2009.02.073.

[16] T. Yoshida, K. Enpuku, F. Ludwig, J. Dieckhoff, T. Wawrzik, A. Lak, and M. Schilling. Characterization of Resovist® Nanoparticles for Magnetic Particle Imaging. In *Springer Proceedings in Physics*, volume 140, pages 3–7, 2012. doi:10.1007/978-3-642-24133-8_1.

[17] D. Eberbeck, C. L. Dennis, N. F. Huls, K. L. Krycka, C. Gruttner, and F. Westphal. Multicore Magnetic Nanoparticles for Magnetic Particle Imaging. *IEEE Trans. Magn.*, 49(1):269–274, 2013. doi:10.1109/TMAG.2012.2226438.

[18] S. Ota and T. Yamada Y. Takemura. Dipole-dipole interaction and its concentration dependence of magnetic fluid evaluated by alternating current hysteresis measurement. *J. Appl. Phys.*, 117 (17):17D713, 2015. doi:10.1063/1.4914061.

[19] F. Ahrentorp, A. Astalan, J. Blomgren, C. Jonasson, E. Wetterskog, P. Svedlindh, A. Lak, F. Ludwig, L. J. van Ijzendoorn, F. Westphal, C. Grüttner, N. Gehrke, S. Gustafsson, E. Olsson, and C. Johansson. Effective particle magnetic moment of multi-core particles. *J. Magn. Magn. Mater.*, 380:221–226, 2015. doi:10.1016/j.jmmm.2014.09.070.

[20] M. Wu, Y. Xiong, Y. Jia, H. Niu, H. Qi, J. Ye, and Q. Chen. Magnetic field-assisted hydrothermal growth of chain-like nanostructure of magnetite. *Chem. Phys. Lett.*, 401(4–6):374–379, 2005. doi:10.1016/j.cplett.2004.11.080.

[21] L. C. Branquinho, M. S. Carrião, A. S. Costa, N. Zufelato, M. H. Sousa, R. Miotto, R. Ivkov, and A. F. Bakuzis. Effect of magnetic dipolar interactions on nanoparticle heating efficiency: Implications for cancer hyperthermia. *Sci. Rep.*, 3:2887, 2013. doi:10.1038/srep02887.

[22] C. Martinez-Boubeta, K. Simeonidis, A. Makridis, M. Angelakeris, O. Iglesias, P. Guardia, A. Cabot, L. Yedra, S. Estradé, F. Peiró, Z. Saghi, P. A. Midgley, Iván Conde-Leborán, D. Serantes, and D. Baldomir. Learning from Nature to Improve the Heat Generation of Iron-Oxide Nanoparticles for Magnetic Hyperthermia Applications. *Sci. Rep.*, 3:1652, 2013. doi:10.1038/srep01652.

[23] S. Ota, R. Kitaguchi, R. Takeda, T. Yamada, and Y. Takemura. Rotation of Magnetization Derived from Brownian Relaxation in Magnetic Fluids of Different Viscosity Evaluated by Dynamic Hysteresis Measurements over a Wide Frequency Range. *Nanomaterials*, 6(9):170, 2016. doi:10.3390/nano6090170.

[24] H. Mamiyama and B. Jeyadevan. Hyperthermic effects of dissipative structures of magnetic nanoparticles in large alternating magnetic fields. *Sci. Rep.*, 1:157, 2011. doi:10.1038/srep00157.

[25] J. Carrey, B. Mehdaoui, and M. Respaud. Simple models for dynamic hysteresis loop calculations of magnetic single-domain nanoparticles: Application to magnetic hyperthermia optimization. *J. Appl. Phys.*, 109(8):083921, 2011. doi:10.1063/1.3551582.

[26] R. E. Rosensweig. Heating magnetic fluid with alternating magnetic field. *J. Magn. Magn. Mater.*, 252:370–374, 2002. doi:10.1016/S0304-8853(02)00706-0.

[27] W. T. Coffey and Y. P. Kalmykov. Thermal fluctuations of magnetic nanoparticles: Fifty years after Brown. *J. Appl. Phys.*, 112(12): 121301, 2012. doi:10.1063/1.4754272.

[28] R. Hergt, R. Hiergeist, M. Zeisberger, G. Glöckl, W. Weitschies, L. P. Ramirez, I. Hilger, and W. A. Kaiser. Enhancement of AC-losses of magnetic nanoparticles for heating applications. *J. Magn. Magn. Mater.*, 280(2–3):358–368, 2004. doi:10.1016/j.jmmm.2004.03.034.

